ATATÜRK ÜNİVERSİTESİ YAYINLARI
ATATURK UNIVERSITY PUBLICATIONS

Research Article DOI: 10.62425/pharmata.1953041

Design and Synthesis of Hybrid Pyrazole-Based Cholinesterase Inhibitors Incorporating *N*-Benzyl and *O*-Benzyl Moieties: Biological and Molecular Docking Studies

Burak KUZU[1]
[1] Van Yüzüncü Yıl University, Faculty of Pharmacy, Department of Pharmaceutical Chemistry, Van, Türkiye

Beyza Nur KARCI[1]
[1] Van Yüzüncü Yıl University, Faculty of Pharmacy, Department of Pharmaceutical Chemistry, Van, Türkiye

Fatih DÖNMEZ[2]
[2] Van Yüzüncü Yıl University, Faculty of Pharmacy, Department of Biochemistry, Van, Türkiye

ABSTRACT

Objective: This study aimed to design, synthesize, and evaluate novel hybrid pyrazole-based cholinesterase inhibitors incorporating *N*-benzyl and *O*-benzyl moieties, combining distinct pharmacophoric features to explore inhibitory activity and binding characteristics against acetylcholinesterase (AChE) and butyrylcholinesterase (BChE).

Methods: A series of hybrid compounds was synthesized via a multi-step synthetic route involving semicarbazone formation, cyclization to pyrazole derivatives, *N*-benzylation, reduction, and final benzylation. Structural characterization was performed using ^{1}H-NMR, ^{13}C-NMR, and HRMS analyses. The inhibitory activities of the synthesized compounds against AChE and BChE were determined using the Ellman method, and IC_{50} values were calculated. Structure-activity relationship (SAR) analysis was conducted to evaluate the impact of structural variations. Molecular docking studies were performed using AutoDock 4.2 to investigate ligand-enzyme interactions and binding modes.

Results: Among the synthesized compounds, PBO-5 exhibited the most potent AChE inhibitory activity, with an IC_{50} value of 0.537 ± 0.006 µM, whereas PBO-2 showed the strongest BChE inhibition, with an IC_{50} value of 0.958 ± 0.005 µM. Under the same experimental conditions, donepezil exhibited IC_{50} values of 0.048 ± 0.002 µM and 2.132 ± 0.035 µM against AChE and BChE, respectively. SAR analysis indicated that variations in the aromatic substituents, together with the *N*-benzyl and *O*-benzyl moieties, influenced cholinesterase inhibitory potency. Molecular docking provided complementary hypotheses regarding the possible binding orientations and non-covalent interactions of the compounds.

Conclusion: These findings support the potential of the hybrid pyrazole scaffold as a useful framework for the further development of cholinesterase inhibitors. The observed structure-activity relationships and favorable enzyme-binding interactions provide a basis for future optimization of this scaffold toward more potent cholinesterase inhibitors.

Keywords: Benzyloxy, Cholinesterase Inhibitors, Molecular Docking, *N*-Benzyl, Pyrazole, Structure- Activity Relationship

Received 16.05.2026
Accepted 26.10.2026
Publication Date 13.11.2026

Corresponding author: Burak KUZU
E-mail: burakkuzu@yyu.edu.tr
Cite this article: Kuzu B, Karcı BN, Dönmez F. Design and Synthesis of Hybrid Pyrazole-Based Cholinesterase Inhibitors Incorporating N-Benzyl and O-Benzyl Moieties: Biological and Molecular Docking Studies. *Pharmata*. 2026;6(3):129-140

Content of this journal is licensed under a Creative Commons Attribution-Noncommercial 4.0 International License.

INTRODUCTION

Alzheimer's disease (AD), one of the most prominent neurodegenerative disorders, is an age-associated form of dementia characterized by progressive cognitive decline, particularly memory impairment. As the disease progresses, not only memory but also executive functions, such as attention, planning, and decision-making, are significantly affected.[1] With the continuous increase in the aging global population, the prevalence of AD is steadily rising, while its pathophysiology remains highly complex and multifactorial. In this context, mechanisms such as amyloid-β accumulation, tau-related pathological alterations, synaptic loss, and neuroinflammation interact directly or indirectly to drive disease progression.[2] Among these, synaptic loss is particularly important, as it can emerge even in the early stages of the disease.

Disruption of synaptic integrity, especially within glutamatergic and cholinergic systems, constitutes the fundamental biological basis of cognitive decline.[3] Accordingly, extensive efforts in medicinal chemistry have focused on the cholinergic hypothesis of AD, aiming to enhance synaptic transmission. In particular, developing novel, target-specific, and effective therapeutic agents that increase acetylcholine (ACh) levels in the synaptic cleft by inhibiting acetylcholinesterase (AChE), the enzyme responsible for ACh hydrolysis, remains at the forefront of current research.[4]

Although AChE is the primary enzyme responsible for acetylcholine hydrolysis, BChE also contributes to cholinergic regulation and may become increasingly relevant during the progression of Alzheimer's disease (AD).[5,6] Therefore, simultaneous targeting of AChE and BChE has been considered a potential strategy for maintaining cholinergic function throughout disease progression.[6] Accordingly, the PBO derivatives were evaluated against both enzymes to investigate their overall cholinesterase inhibitory potential and enzyme-dependent activity profiles.

Although numerous therapeutic agents have been developed as anticholinesterase inhibitors for the treatment of AD, only a limited number have reached clinical use. This is primarily due to severe and sometimes treatment-limiting side effects associated with long-term administration. For instance, tacrine was withdrawn from clinical use because of its hepatotoxicity risk.[7] Currently approved drugs by the U.S. Food and Drug Administration (FDA), such as Rivastigmine, Galantamine, and Donepezil, are also known to cause various adverse effects upon prolonged use.[8] These limitations indicate that existing pharmacological options are insufficient to halt disease progression and are largely restricted to symptomatic relief. Indeed, despite the increasing prevalence of AD, current therapeutic strategies fail to fully meet clinical needs.[9] Therefore, a significant focus of contemporary medicinal chemistry research is the development of safer, more selective, and target-specific agents through modern design strategies.

Donepezil, one of the most widely used drugs in AD treatment, effectively binds to the active-site pocket of AChE by simultaneously targeting two distinct domains within the catalytic site.[10,11] Extensive structure-activity relationship (SAR) studies have demonstrated that the 3.4-dimethoxyindanone scaffold provides an aromatic core that contributes to π-π interactions, while the *N*-benzylpiperidine moiety serves as a basic center that interacts with the enzyme's anionic site, thereby enabling AChE inhibition.[12] Based on these findings, subsequent research has focused on the design of novel, more potent AChE inhibitors while preserving key pharmacophoric features. For instance, in a study where the *N*-benzylpiperidine motif was retained, and the indanone ring was modified with aryl or heteroaryl groups, a pyrazole-derived compound (1) exhibited AChE inhibitory activity with an IC_{50} value of 5.94 ± 1.08 µM.[13] In another study employing a similar design strategy with an isoxazole ring, compound (2) displayed an IC_{50} value of 15.16 µM (Figure 1A).[14] The *N*-benzylpiperidine motif has been utilized not only in classical hybrid designs but also as an effective building block in fragment-based approaches. Indole (3) and pyrrole (4) derivatives modified via *N*-benzylation exhibited AChE inhibitory activities with IC_{50} values of 0.3 µM and 18.67 µM, respectively.[15,16] The presence of *O*- or *N*-benzyloxy groups on the aromatic core of these compounds offers an alternative design strategy. Indeed, a benzyloxy-substituted derivative (5) was reported to have an IC_{50} value of 0.625 µM, while a dibenzyloxy derivative (6), designed based on this scaffold, demonstrated AChE inhibitory potential in *in silico* studies.[17] Furthermore, another compound (7), in which two pyrazole rings are linked via a -CH_2-NH-CH_2- bridge, exhibited remarkable inhibitory activity with an IC_{50} value of 0.35 µM and was proposed as a lead structure (Figure 1B).[18]

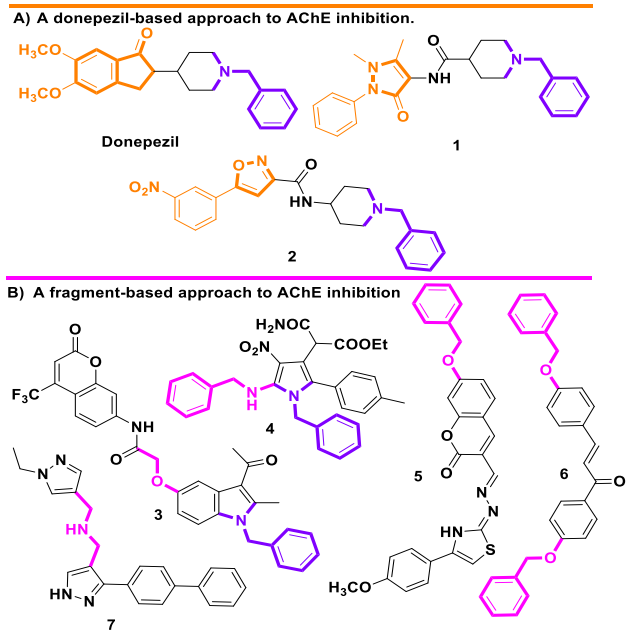

Figure 1. Design strategies and representative examples of AChE inhibitors: (A) donepezil-based designs, (B) fragment-based designs.

Collectively, these findings suggest that AChE inhibitors can generally be classified into two main categories. The first class reflects a donepezil-based design approach, where an aromatic core is linked to an *N*-benzyl motif via a suitable linker. The second class represents an alternative strategy in which both the *N*-benzyl motif and *O*- or *N*-benzyl derivatives are substituted onto a central aromatic ring (Figure 2).

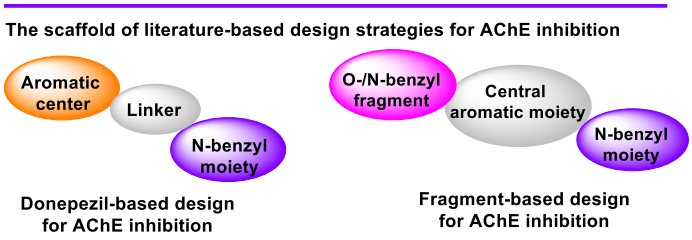

Figure 2. The scaffold of literature-based design strategies for AChE inhibition.

This study aimed to develop and synthesize a series of pyrazole-based derivatives incorporating selected structural features identified in previously reported cholinesterase inhibitors. The designed compounds were synthesized, purified using appropriate chromatographic techniques, and structurally characterized by ^{1}H NMR, ^{13}C NMR, and HRMS analyses. Their inhibitory activities against AChE and BChE were evaluated *in vitro* using enzyme inhibition assays, with donepezil as the reference compound, and the corresponding IC_{50} values were determined. Structure-activity relationship (SAR) analyses were subsequently performed to assess the relationship between the structural modifications and cholinesterase inhibitory activity. Additionally, molecular docking studies were conducted to investigate the potential interaction profiles and binding modes of the synthesized compounds within the active sites of AChE and BChE. Overall, this study explores a literature-guided molecular hybridization strategy for developing pyrazole-based cholinesterase inhibitors and provides experimental and computational insights into their structure-activity relationships.

METHODS

Synthesis of Semicarbazone Derivatives

Sodium acetate (1.3 mmol) and semicarbazide hydrochloride (1 mmol) were dissolved in ethanol (15 mL). The reaction mixture was stirred at room temperature for 15 min, then aromatic acetyl derivatives (1 mmol) were added. The resulting mixture was refluxed at 80 °C for 6 h. Upon completion, the reaction mixture was cooled to room temperature and poured into an ice-water mixture (50 mL), yielding white solid particles. The suspension was stirred for an additional 15 min, filtered, and the collected solid was air-dried at room temperature. The crude product was used in the next step without further purification.[19]

Synthesis of Carboxaldehyde-Substituted Pyrazole Derivatives

Semicarbazone derivatives (1 mmol) obtained from the previous step were dissolved in dry DMF (5 mL) and cooled in an ice bath. Phosphoryl chloride ($POCl_3$, 2.2 mmol) was added dropwise, and the reaction mixture was stirred at 0 °C for 30 min. Subsequently, the mixture was heated to 65 °C and stirred for 6 h. After confirming the complete consumption of the starting material, the mixture was cooled to room temperature and poured into an ice-water mixture (50 mL). The solution was neutralized with 2 N NaOH, and a solid precipitate formed at pH 7-8. The resulting solid was filtered, washed with water, and air-dried overnight at room temperature. The crude product was used directly in the next step without further purification. The procedure was adapted from the reported methods.[20,21]

Synthesis of *N*-Benzyl-Substituted Pyrazole Derivatives

Carboxaldehyde-substituted pyrazole derivatives (1 mmol) were dissolved in DMF (7 mL). While stirring, potassium carbonate (2 mmol) was added, and the mixture was stirred for 30 min at 25 °C. Subsequently, benzyl bromide (1.2 mmol) was added dropwise. The reaction mixture was stirred at room temperature for 4 h, and the progress was monitored by TLC. Upon completion, the crude products were extracted using saturated brine solution (50 mL) and ethyl acetate (3×30 mL), followed by purification via column chromatography using an appropriate mobile phase (ethyl acetate/n-hexane).[22]

Synthesis of *N*-Benzyl-Pyrazole-Methanol Derivatives

Carboxaldehyde-substituted *N*-benzyl-pyrazoles (1 mmol) were dissolved in ethanol (10 mL), and sodium borohydride (2 mmol) was added. The reaction mixture was stirred at 25 °C for 6 h. Reaction completion was monitored by TLC, and the mixture was then poured into an ice-water mixture (50 mL). The suspension was stirred for an additional 15 min, filtered, and the solid product was air-dried at room temperature. The crude product was used in the next step without further purification.[23]

Synthesis of Target Hybrid Derivatives

Pyrazole-methanol derivatives (1 mmol) obtained from the previous step were dissolved in DMF (7 mL). While stirring, potassium carbonate (2 mmol) was added, and the mixture was stirred for 30 min. Benzyl bromide (1.2 mmol) was then added dropwise, and the reaction was continued at room

temperature for 4 h with TLC monitoring. Upon completion, the crude products were extracted with saturated brine (50 mL) and ethyl acetate (3 × 30 mL), then purified by column chromatography using an appropriate mobile phase (ethyl acetate/n-hexane).[22]

Characterizations of Target Hybrid Derivatives

1-Benzyl-4-((benzyloxy)methyl)-3-phenyl-1H-pyrazole (PBO-1): Light brown viscous liquid, yield: 84%, Rf: 0.70 (ethyl acetate/n-hexane, 1/6).^{1}H NMR (400 MHz, $CDCl_3$) δ 7.77-7.75 (m, 2H, Ar-H), 7.39-7.24 (m, 14H, Ar-H), 5.32 (s, 2H, N-CH_2-), 4.56 (s, 2H, O-CH_2-), 4.48 (s, 2H, O-CH_2-).^{13}C NMR (100 MHz, $CDCl_3$) δ 150.8, 138.0, 136.2, 133.2, 131.2, 128.8, 128.5, 128.4, 128.1, 128.0, 128.9, 127.8, 127.7, 127.6, 115.9, 72.1, 62.8, 56.1. HRMS $[M+H]^+$; Calculated for $C_{24}H_{23}N_2O^+$: 355.1804, Found: 355.1808.

1-Benzyl-4-((benzyloxy)methyl)-3-(4-fluorophenyl)-1H-pyrazole (PBO-2)*:* Light yellow viscous liquid, yield: 63%, Rf: 0.75 (ethyl acetate/n-hexane, 1/6).^{1}H NMR (400 MHz, $CDCl_3$) δ 7.78-7.75 (m, 2H, Ar-H), 7.40-7.37 (m, 3H, Ar-H), 7.37-7.32 (m, 5H, Ar-H), 7.32-7.28 (m, 3H, Ar-H), 7.08 (t, J= 8.6 Hz, 2H, Ar-H), 5.32 (s, 2H, N-CH_2-), 4.57 (s, 2H, O-CH_2-), 4.45 (s, 2H, O-CH_2-).^{13}C NMR (100 MHz, $CDCl_3$) δ 162.5 (d, J= 246.5 Hz), 150.1, 137.9, 136.2, 131.4, 129.5 (d, J= 8.0 Hz), 129.4 (d, J= 3.1 Hz), 128.9, 128.5, 128.1, 128.0, 127.8, 127.7, 115.6, 115.4 (d, J= 21.3 Hz), 72.1, 62.5, 56.1. HRMS $[M+H]^+$; Calculated for $C_{24}H_{22}FN_2O^+$: 373.1710, Found: 373.1713.

1-Benzyl-4-((benzyloxy)methyl)-3-(4-chlorophenyl)-1H-pyrazole (PBO-3): Yellow viscous liquid, yield: 92%, Rf: 0.65 (ethyl acetate/n-hexane, 1/6).^{1}H NMR (400 MHz, $CDCl_3$) δ 7.74-7.71 (m, 2H, Ar-H), 7.39-7.26 (m, 13H, Ar-H), 5.31 (s, 2H, N-CH_2-), 4.56 (s, 2H, O-CH_2-), 4.44 (s, 2H, O-CH_2-).^{13}C NMR (100 MHz, $CDCl_3$) δ 149.8, 137.8, 136.0, 133.5, 131.7, 131.5, 129.0, 128.9, 128.6, 128.5, 128.2, 128.1, 128.0, 127.9, 115.8, 72.1, 62.5, 56.2. HRMS $[M+H]^+$; Calculated for $C_{24}H_{22}ClN_2O^+$: 389.1415, Found: 389.1415.

1-Benzyl-4-((benzyloxy)methyl)-3-(4-bromophenyl)-1H-pyrazole (PBO-4): Light brown viscous liquid, yield: 93%, Rf: 0.60 (ethyl acetate/n-hexane, 1/6).^{1}H NMR (400 MHz, $CDCl_3$) δ 7.68-7.55 (m, AA'BB' system, 2H, Ar-H), 7.52-7.50 (m, AA'BB' system, 2H, Ar-H), 7.40-7.24 (m, 11H, Ar-H), 5.31 (s, 2H, N-CH_2-), 4.56 (s, 2H, O-CH_2-), 4.44 (s, 2H, O-CH_2-).^{13}C NMR (100 MHz, $CDCl_3$) δ 149.8, 137.8, 136.0, 132.2, 131.6, 131.5, 129.4, 128.9, 128.5, 128.2, 128.1, 128.0, 127.9, 121.8, 115.9, 72.1, 62.5, 56.2. HRMS $[M+H]^+$; Calculated for $C_{24}H_{22}BrN_2O^+$: 433.0910, Found: 433.0916.

1-Benzyl-4-((benzyloxy)methyl)-3-(p-tolyl)-1H-pyrazole (PBO-5): Light brown viscous liquid, yield: 75%, Rf: 0.80 (ethyl acetate/n-hexane, 1/6).^{1}H NMR (400 MHz, $CDCl_3$) δ 7.87-7.85 (m, AA'BB' system, 2H, Ar-H), 7.50-7.44 (m, 7H, Ar-H), 7.42-7.35 (m, 6H, Ar-H), 5.37 (s, 2H, N-CH_2-), 4.66 (s, 2H, O-CH_2-), 4.59 (s, 2H, O-CH_2-), 2.48 (s, 3H, Ar-CH_3).^{13}C NMR (100 MHz, $CDCl_3$) δ 151.0, 138.2, 137.4, 136.5, 131.4, 130.7, 129.4, 128.9, 128.6, 128.2, 128.0, 127.9, 127.8, 127.8, 115.9, 72.2, 63.0, 56.1, 21.5. HRMS $[M+H]^+$; Calculated for $C_{25}H_{25}N_2O^+$: 369.1961, Found: 369.1966.

1-Benzyl-4-((benzyloxy)methyl)-3-(4-(trifluoromethyl)phenyl)-1H-pyrazole (PBO-6): Light brown viscous liquid, yield: 55%, Rf: 0.85 (ethyl acetate/n-hexane, 1/6).^{1}H NMR (400 MHz, $CDCl_3$) δ 7.99-7.97 (m, AA'BB' system, 2H, Ar-H), 7.69-7.67 (m, AA'BB' system, 2H, Ar-H), 7.45-7.32 (m, 11H, Ar-H), 5.35 (s, 2H, N-CH_2-), 4.61 (s, 2H, O-CH_2-), 4.51 (s, 2H, O-CH_2-).^{13}C NMR (100 MHz, $CDCl_3$) δ 149.4, 137.8, 136.9, 136.0, 131.7, 129.5, 128.9, 128.6, 128.3, 128.2, 128.0, 127.94, 127.92, 125.8, 125.4 (q, J= 3.7 Hz), 116.4, 72.2, 62.5, 56.3. HRMS $[M+H]^+$; Calculated for $C_{25}H_{22}F_3N_2O^+$: 423.1678, Found: 423.1682.

1-Benzyl-4-((benzyloxy)methyl)-3-(4-methoxyphenyl)-1H-pyrazole (PBO-7): Light yellow viscous liquid, yield: 68%, Rf: 0.55 (ethyl acetate/n-hexane, 1/6).^{1}H NMR (400 MHz, $CDCl_3$) δ 7.73-7.71 (m, AA'BB' system, 2H, Ar-H), 7.43-7.22 (m, 11H, Ar-H), 6.95-6.93 (m, AA'BB' system, 2H, Ar-H), 5.31 (s, 2H, N-CH_2-), 4.56 (s, 2H, O-CH_2-), 4.47 (s, 2H, O-CH_2-), 3.83 (s, 3H, Ar-OCH_3).^{13}C NMR (100 MHz, $CDCl_3$) δ 159.2, 150.8, 138.0, 136.3, 131.2, 129.1, 128.8, 128.5, 128.1, 127.9, 127.8, 127.7, 126.0, 115.4, 113.9, 72.0, 62.8, 56.0, 55.3. HRMS $[M+H]^+$; Calculated for $C_{25}H_{25}N_2O_2^+$: 385.1910, Found: 385.1915.

1-Benzyl-4-((benzyloxy)methyl)-3-(3.4-dimethoxyphenyl)-1H-pyrazole (PBO-8): Yellow viscous liquid, yield: 71%, Rf: 0.45 (ethyl acetate/n-hexane, 1/6).^{1}H NMR (400 MHz, $CDCl_3$) δ 7.40 (s, 1H, Ar-H), 7.36-7.24 (m, 12H, Ar-H), 6.88 (d, J= 8.3 Hz, 1H, Ar-H), 5.31 (s, 2H, N-CH_2-), 4.55 (s, 2H, O-CH_2-), 4.46 (s, 2H, O-CH_2-), 3.90 (s, 3H, Ar-OCH_3), 3.86 (s, 3H, Ar-OCH_3).^{13}C NMR (100 MHz, $CDCl_3$) δ 150.9, 148.8, 148.7, 138.0, 136.2, 131.3, 128.8, 128.4, 128.1, 128.0, 127.9, 127.7, 126.1, 120.3, 115.4, 111.0, 71.9, 62.8, 56.0, 55.9, 55.8. HRMS $[M+H]^+$; Calculated for $C_{26}H_{27}N_2O_3^+$: 415.2016, Found: 415.2020.

1-Benzyl-4-((benzyloxy)methyl)-3-(naphthalen-2-yl)-1H-pyrazole (PBO-9): Light yellow viscous liquid, yield: 82%, Rf: 0.50 (ethyl acetate/n-hexane, 1/6).^{1}H NMR (400 MHz, $CDCl_3$) δ 8.35 (s, 1H, Ar-H), 8.06-8.04 (m, 1H, Ar-H), 7.95-7.90 (m, 3H, Ar-H), 7.53-7.34 (m, 13H, Ar-H), 5.39 (s, 2H, N-

CH_2-), 4.67 (s, 2H, O-CH_2-), 4.60 (s, 2H, O-CH_2-).^{13}C NMR (100 MHz, $CDCl_3$) δ 150.9, 138.1, 136.3, 133.6, 132.9, 131.5, 130.9, 128.9, 128.6, 128.4, 128.2, 128.1, 128.0, 127.8, 127.7, 126.8, 126.1, 126.0, 125.9, 72.2, 63.1, 56.2. HRMS $[M+H]^+$; Calculated for $C_{28}H_{25}N_2O^+$: 405.1961, Found: 405.1965.

1-Benzyl-3-([1.1'-biphenyl]-4-yl)-4-((benzyloxy)methyl)-1H-pyrazole (PBO-10): Brown viscous liquid, yield: 80%, Rf: 0.55 (ethyl acetate/n-hexane, 1/6).^{1}H NMR (400 MHz, $CDCl_3$) δ 7.98-7.97 (m, AA'BB' system, 2H, Ar-H), 7.73-7.71 (m, 4H, Ar-H), 7.53-7.34 (m, 14H, Ar-H), 5.53 (s, 2H, N-CH_2-), 4.65 (s, 2H, O-CH_2-), 4.59 (s, 2H, O-CH_2-).^{13}C NMR (100 MHz, $CDCl_3$) δ 150.5, 140.9, 140.3, 138.1, 136.4, 132.4, 131.5, 128.9, 128.8, 128.6, 128.3, 128.2, 128.0, 127.8, 127.7, 127.4, 127.3, 127.1, 116.1, 72.1, 62.9, 56.2. HRMS $[M+H]^+$; Calculated for $C_{30}H_{27}N_2O^+$: 431.2117, Found: 431.2123.

In Vitro AChE and BChE Inhibition Assay

The inhibitory effects of the synthesized compounds against AChE (from *Electrophorus electricus*) and BChE (from equine serum) were evaluated according to the method described by Ellman et al.[24]. Briefly, 785 µL of phosphate buffer (0.1 M, pH 8), 5 µL of test compound solution (prepared at different concentrations in DMSO), 100 µL of DTNB (5 mM), and 10 µL of enzyme solution (1 U/mL for AChE and 2 U/mL for BChE) respectively, were combined and incubated for 15 min at 25 ± 1 °C. The reaction was then initiated by adding 100 µL of substrate solution (5 mM; acetylthiocholine iodide for AChE and butyrylthiocholine iodide for BChE), and absorbance was recorded at 412 nm for 3 min at 25 ± 1 °C. The final DMSO concentration was maintained at 0.5% (v/v) across all experimental groups. For each concentration, blanks were prepared by replacing the enzyme solution with an equal volume of phosphate buffer and subjected to the same procedures to correct for absorbance contributions from the test compounds and the standard inhibitor (donepezil). All measurements were performed in technical triplicate. After blank correction, the change in absorbance (ΔA) was calculated by subtracting the initial absorbance from the absorbance at the end of the 3 min measurement period. The activity of the inhibitor-free control was set at 100%, and percentage enzyme activity was calculated using the following equation. A separate concentration-response curve was generated for each technical replicate. IC_{50} values for the compounds and the standard inhibitor were calculated by fitting these curves using nonlinear regression ([Inhibitor] vs. normalized response - variable slope) in GraphPad Prism 8 (GraphPad Software, San Diego, CA, USA) and were reported as the mean ± standard deviation of the values obtained from the three replicates.

$$\text{Enzyme activity (\%)} = (\Delta A_{Sample} / \Delta A_{Control}) \times 100$$

Here, ΔA_{Sample} represents the change in absorbance of the reaction containing the test compound or standard inhibitor, and $\Delta A_{Control}$ represents the change in absorbance of the inhibitor-free control reaction.

Molecular Docking Studies

Molecular docking studies were performed using AutoDock 4.2 to investigate the interactions between the synthesized compounds and the hAChE and hBChE enzymes. The three-dimensional structures of the enzymes were obtained from the RCSB Protein Data Bank (www.rcsb.org) using PDB IDs 7E3H and 4BDS, respectively. The 7E3H structure is an X-ray crystal structure of hAChE complexed with the co-crystallized inhibitor donepezil, determined at 2.45 Å resolution, whereas the 4BDS structure is an X-ray crystal structure of hBChE complexed with tacrine, determined at 2.10 Å resolution.[25,26] These structures were selected because they represent experimentally determined human cholinesterase structures with structurally characterized inhibitor-bound active sites, providing suitable models for investigating the binding modes of the synthesized PBO derivatives.

The molecular structures of the target compounds were drawn using GaussView 5.0 and optimized using Density Functional Theory (DFT) calculations with the Gaussian 03 package. Geometry optimizations were performed at the B3LYP/6-31G(d) level. For protein preparation, the co-crystallized ligands and water molecules were removed, polar hydrogens were added, and Kollman atomic charges were assigned to the protein structures. The co-crystallized ligands, namely donepezil for hAChE and tacrine for hBChE, were initially used to define the corresponding binding sites and were subsequently removed before docking. The protonation and tautomeric states of the ligands were retained as prepared. Gasteiger charges were calculated for the ligands, and rotatable bonds were defined. The protein structures were kept rigid, whereas the ligands were treated as flexible during docking. For hAChE (PDB ID: 7E3H), a grid box of 50 × 50 × 50 points was centered at x = -43.936, y = 36.272, and z = -28.932. For hBChE (PDB ID: 4BDS), a grid box of 50 × 50 × 50 points was centered at x = 132.594, y = 114.497, and z = 43.514. The grid spacing was set to 0.375 Å. These grid parameters were used consistently for the docking simulations of the synthesized compounds and the corresponding co-crystallized inhibitors. To validate the docking protocol, we re-docked the co-crystallized inhibitors into the active sites of AChE and BChE and superimposed the resulting conformations with the corresponding experimental crystal structures.

The calculated RMSD values were 0.70 Å for donepezil in hAChE and 0.04 Å for tacrine in hBChE, supporting the ability of the docking protocol to reproduce the experimentally observed binding modes. Docking simulations were performed using the Lamarckian Genetic Algorithm, with 10 independent runs and a population size of 300. The pose with the lowest predicted binding energy was selected for subsequent interaction analysis. The corresponding protein-ligand complex was then analyzed. Two- and three-dimensional visualizations and detailed interaction analyses of the protein-ligand complexes were performed using Discovery Studio 4.1.[27]

RESULTS

Design Rationale

The reported inhibitory potential of heteroaryl and benzyloxy-containing derivatives in the literature inspired us to develop a new class of cholinesterase inhibitors. A detailed evaluation of previous studies led us to integrate two complementary design strategies into a single hybrid molecular framework. The first strategy was inspired by donepezil, in which an aromatic region contributes to interactions within the AChE active-site gorge, while the second involved incorporating *N*-benzyl and benzyloxy fragments into aromatic or heteroaromatic scaffolds. In the present design, these structural features were combined on a central pyrazole scaffold, with an *N*-benzyl motif and an *O*-benzyl-containing fragment positioned within the same molecular framework, while additional aromatic groups were introduced to provide structural diversification.

To investigate this structural hypothesis, the pyrazole ring was selected as the central scaffold because of its established pharmacological relevance and its suitability for structural modification. *N*-benzylation of the pyrazole nucleus was employed to incorporate the benzyl-based structural feature identified in previously reported cholinesterase inhibitors, whereas the benzyloxy group was introduced to provide an additional aromatic fragment and potentially promote hydrophobic and π-related interactions within the enzyme active site. The aromatic region was further diversified using the dimethoxy-substituted aromatic region of donepezil, together with para-substituted phenyl, naphthyl, and biphenyl moieties (Figure 3). This systematic variation was intended to examine how changes in the size, electronic properties, and hydrophobic character of the aromatic substituent influence AChE and BChE inhibitory activity.

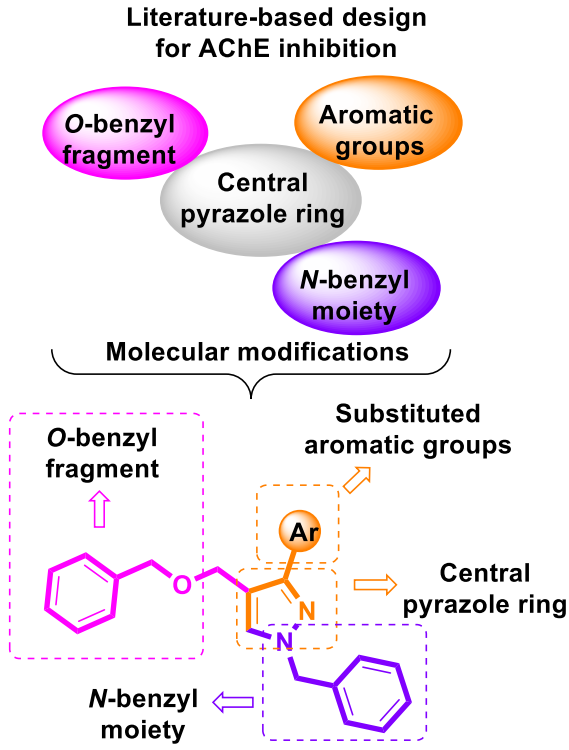

Figure 3. Design strategy for cholinesterase inhibitors.

Thus, the molecular hybridization strategy employed in this study combined complementary structural features from previously reported cholinesterase inhibitors rather than reproducing a single known pharmacophore. The resulting compounds were designed as a pyrazole-centered framework containing *N*-benzyl and benzyloxy structural elements, along with a variable aromatic region. This design was subsequently evaluated experimentally through AChE and BChE inhibition assays and further investigated by molecular docking to examine the potential binding modes of the synthesized compounds.

Chemistry

The target hybrid pyrazole derivatives were synthesized through a stepwise, modular strategy, enabling efficient construction of structurally diverse compounds from readily accessible starting materials (Figure 4).

The overall approach was designed to combine straightforward transformations with minimal intermediate purification, thereby streamlining the synthetic workflow. The sequence was initiated by the formation of semicarbazone intermediates via condensation of aryl methyl ketone derivatives with semicarbazide.

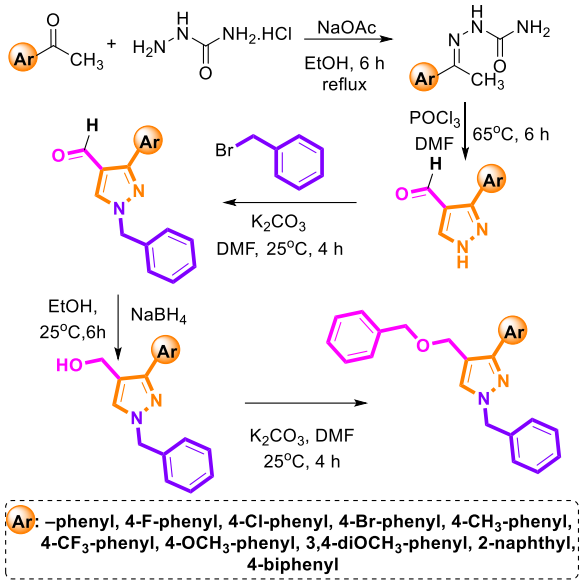

Figure 4. Synthesis of hybrid pyrazole derivatives via Vilsmeier-Haack reaction, *N*-alkylation, and *O*-alkylation.

This transformation provided a convenient entry point for subsequent ring construction. The resulting intermediates were subjected directly to cyclization under Vilsmeier-Haack reaction conditions, yielding pyrazole cores bearing a formyl group. This step represents a key transformation in the synthetic route, as it establishes the heterocyclic scaffold central to the target structures. The obtained pyrazole aldehydes were then diversified via *N*-alkylation, introducing benzyl substituents at the pyrazole nitrogen. In parallel, the aldehyde functionality served as a versatile handle for further derivatization. Selective conversion of this group into the corresponding alcohol was achieved via sodium borohydride reduction, furnishing pyrazole-methanol intermediates without affecting the integrity of the heterocyclic core. In the final stage, these alcohol derivatives were further functionalized via *O*-alkylation, thereby introducing an additional benzyl moiety and affording the desired hybrid compounds. This dual-functionalization strategy, involving nitrogen and oxygen alkylation, proved effective in enhancing molecular complexity and structural diversity.

The synthesized hybrid pyrazole derivatives (**PBO1-10**) were obtained in moderate to excellent yields (55-93%), confirming the efficiency and general applicability of the developed synthetic strategy. All compounds were isolated as viscous liquids with varying colors ranging from light yellow to brown, and exhibited good chromatographic behavior (R_f = 0.45-0.85) under the selected solvent system. Structural elucidation of the compounds was achieved by ^{1}H NMR, ^{13}C NMR, and HRMS analyses. In the ^{1}H NMR spectra, all derivatives consistently displayed characteristic singlet signals corresponding to the benzylic methylene protons. The *N*-CH_2 group appeared around δ 5.3 ppm, while the O-CH_2 protons were observed as distinct singlets in the δ 4.4–4.7 ppm region, confirming successful *N*-alkylation and *O*-alkylation. Aromatic protons were distributed over the expected δ 6.8-8.3 ppm range, with splitting patterns consistent with the substitution profiles of the phenyl rings. The ^{13}C NMR spectra further supported the proposed structures, with characteristic signals for aromatic carbons and diagnostic peaks corresponding to methylene carbons (δ 56-72 ppm). Substituent-specific signals were also observed, such as the CF_3 carbon (quartet) and C-F coupling in fluorinated derivatives, as well as methoxy carbons in methoxy-substituted analogs. High-resolution mass spectrometry (HRMS) data confirmed the molecular compositions of all compounds, with experimentally observed $[M+H]^+$ values in excellent agreement with the calculated masses, thereby supporting the assigned molecular formulas and structural identities.

In Vitro AChE and BChE Inhibition Assay

The synthesized pyrazole-based derivatives (**PBO1-10**) were evaluated for their inhibitory activities against acetylcholinesterase (AChE) and butyrylcholinesterase (BChE) using *in vitro* enzymatic assays. Donepezil was used as the reference drug under identical experimental conditions. The inhibitory potencies were expressed as IC_{50} values (µM), and the obtained results are summarized in Table 1.

Table 1. *In vitro* AChE and BChE inhibitory activities of synthesized **PBO** derivatives and Donepezil expressed as IC_{50} values (µM).

	AChE		BChE	
Entry	**IC_{50} (µM)**	**R^2**	**IC_{50} (µM)**	**R^2**
PBO-1	6.520 ± 0.093	0.993	1.777 ± 0.049	0.991
PBO-2	6.011 ± 0.079	0.992	0.958 ± 0.005	0.991
PBO-3	5.430 ± 0.049	0.993	2.768 ± 0.114	0.990
PBO-4	1.131 ± 0.027	0.998	1.227 ± 0.023	0.992
PBO-5	0.537 ± 0.006	0.999	1.092 ± 0.007	0.996
PBO-6	0.615 ± 0.008	0.997	3.473 ± 0.102	0.992
PBO-7	1.336 ± 0.016	0.998	1.459 ± 0.018	0.998
PBO-8	1.436 ± 0.023	0.992	1.162 ± 0.009	0.999
PBO-9	0.785 ± 0.006	0.999	3.238 ± 0.132	0.990
PBO-10	2.676 ± 0.021	0.990	4.531 ± 0.030	0.987
Donepezil	0.048 ± 0.002	0.996	2.132 ± 0.035	0.993

The nonlinear regression models showed high goodness-of-fit values, with R^2 values ranging from 0.987 to 0.999. These values describe the fit of the concentration-response curves but should not be interpreted as independent evidence of assay reproducibility. Although none of the synthesized compounds surpassed donepezil against AChE, several derivatives demonstrated superior BChE inhibition,

suggesting that the designed scaffold may represent a promising structural framework for the development of multifunctional cholinesterase inhibitors for Alzheimer's disease therapy.

Molecular Docking Analyses

To further investigate the molecular basis of the observed cholinesterase inhibitory activities, molecular docking studies were performed against human acetylcholinesterase (hAChE, PDB ID: 7E3H) and human butyrylcholinesterase (hBChE, PDB ID: 4BDS). The docking analyses were performed to evaluate the possible binding orientations, predicted binding affinities, and key intermolecular interactions of the synthesized PBO derivatives within the binding sites of both enzymes. Table 2 summarizes the docking results.

Table 2. Docking results of the compounds against hAChE and hBChE.

Entry	hAChE (PDB ID: 7E3H)		hBChE (PDB ID: 4BDS)	
	Predicted Binding energy (kcal/mol)	RMSD* (Å)	Predicted Binding energy (kcal/mol)	RMSD* (Å)
PBO-1	-9.39	0.04	-8.57	0.14
PBO-2	-8.78	0.19	-7.86	0.29
PBO-3	-8.88	0.11	-8.37	0.42
PBO-4	-8.89	0.10	-8.09	0.29
PBO-5	-9.08	0.15	-8.01	0.55
PBO-6	-8.82	0.12	-7.42	0.49
PBO-7	-10.32	0.02	-8.20	0.07
PBO-8	-9.97	0.03	-9.42	0.23
PBO-9	-8.22	0.22	-7.86	0.25
PBO-10	-8.88	0.25	-8.51	0.58
Donepezil	-8.26	0.70	-8.47	0.74

*RMSD values represent the deviation of the generated docking poses within the corresponding clusters relative to the lowest-energy pose.

The reliability of the docking protocol was assessed by re-docking the co-crystallized ligands into their respective binding sites. Donepezil was re-docked into hAChE (PDB ID: 7E3H) with a heavy-atom RMSD of 0.70 Å, while tacrine was re-docked into hBChE (PDB ID: 4BDS) with an RMSD of 0.04 Å. These redocking RMSD values, both below the commonly accepted 2.0 Å threshold, support the ability of the docking protocol to reproduce the experimentally observed binding orientations of the co-crystallized inhibitors. Overall, the synthesized derivatives exhibited favorable binding energies for both cholinesterases, with several compounds showing more negative predicted energies than donepezil. Although docking scores did not correlate with experimentally determined IC_{50} values, the docking studies provided valuable structural insights into ligand-enzyme recognition and the intermolecular interactions that may contribute to inhibitory activity.

DISCUSSION

Chemistry

The developed synthetic strategy proved to be efficient, flexible, and broadly applicable for the construction of hybrid pyrazole derivatives. The use of a modular sequence enabled the incorporation of various substituents without requiring extensive purification of intermediates, significantly simplifying the overall workflow. The key cyclization step via the Vilsmeier-Haack reaction was crucial for establishing the pyrazole core and proceeded smoothly across different substrates. Subsequent functionalization steps, including *N*-alkylation and *O*-alkylation, were achieved efficiently, highlighting the compatibility of the reaction conditions with a variety of functional groups. Variations in substituents influenced the isolated yields, with electron-withdrawing groups (e.g., halogens, CF_3) and bulky aromatic systems generally yielding slightly lower amounts than unsubstituted or electron-donating analogs. Nevertheless, all derivatives were obtained in synthetically useful yields, demonstrating the robustness of the protocol. Spectroscopic data consistently confirmed the success of each transformation step, particularly the presence of diagnostic methylene signals and substituent-specific features in NMR spectra. The good agreement between the calculated and observed HRMS values further supported the proposed molecular compositions and structural assignments of the synthesized compounds. Overall, the results show that this synthetic approach provides a reliable platform for rapidly generating structurally diverse pyrazole-based hybrids, making it well suited for further applications in medicinal chemistry and structure-activity relationship studies.

In Vitro AChE and BChE Inhibition Assay

The tested compounds exhibited considerable inhibitory activity against both cholinesterase enzymes, with IC_{50} values ranging from 0.537 to 6.520 µM for AChE and from 0.958 to 4.531 µM for BChE. Each compound displayed a distinct inhibition profile toward AChE and BChE, as summarized in Table 1. Among the tested compounds, PBO-5 emerged as the most potent AChE inhibitor with an IC_{50} value of 0.537 µM, followed by PBO-6 (0.615 µM) and PBO-9 (0.785 µM). In contrast, PBO-2 exhibited the strongest BChE inhibitory activity, with an IC_{50} of 0.958 µM, outperforming the reference drug, donepezil (IC_{50} = 2.132 µM). Notably, several compounds, including PBO-4, PBO-5, PBO-7, and PBO-8, exhibited inhibitory activity against both enzymes, indicating a dual-inhibition profile.

Structure-Activity Relationship (SAR)

Structure-activity relationship (SAR) analysis revealed that substituents on the aryl moiety of the pyrazole scaffold substantially influenced both AChE and BChE inhibitory activities. The unsubstituted phenyl derivative PBO-1 exhibited moderate inhibitory activity against both AChE (IC_{50} = 6.520 µM) and BChE (IC_{50} = 1.777 µM), indicating that the parent scaffold possesses inherent cholinesterase inhibitory potential. Introducing halogen substituents produced distinct enzyme-dependent activity profiles. The fluoro-substituted derivative PBO-2 showed improved BChE inhibition (IC_{50} = 0.958 µM) compared with PBO-1, whereas its AChE activity remained comparable (IC_{50} = 6.011 µM). Increasing the halogen size from fluorine to chlorine in PBO-3 modestly improved AChE inhibition (IC_{50} = 5.430 µM) but reduced BChE inhibition (IC_{50} = 2.768 µM). Notably, replacing chlorine with bromine in PBO-4 markedly improved AChE inhibition (IC_{50} = 1.131 µM) while maintaining moderate BChE inhibition (IC_{50} = 1.227 µM). These findings suggest that both the electronic and steric characteristics of the halogen substituent contribute to the enzyme-dependent activity profile, although the observed effects cannot be attributed to a single physicochemical parameter. Among the derivatives, the para-methyl-substituted compound PBO-5 exhibited the highest AChE inhibitory activity (IC_{50} = 0.537 µM), representing a substantial improvement over the unsubstituted PBO-1. This finding suggests that incorporation of a moderately lipophilic methyl group may favor hydrophobic accommodation within the AChE gorge. Consistent with this observation, PBO-5 also displayed a favorable docking score of -9.08 kcal/mol and established several interactions with residues lining the hAChE active-site gorge. In contrast, the trifluoromethyl-containing PBO-6 also showed strong AChE inhibition, whereas its BChE activity was considerably weaker, suggesting that the steric and electronic characteristics of the CF_3 group may be less favorable for productive binding in BChE.

Methoxy-substituted derivatives PBO-7 and PBO-8 displayed relatively balanced inhibitory profiles against both enzymes. In particular, PBO-8 retained potent BChE inhibition, suggesting that additional methoxy substitution may provide favorable interactions within the BChE binding site. Expansion of the aromatic system further altered the activity profile. The naphthyl-containing PBO-9 exhibited strong AChE inhibition (IC_{50} = 0.785 µM), which may be associated with increased hydrophobic and π–π interactions within the aromatic-rich enzyme gorge. However, its weaker BChE activity indicates that increased aromatic surface area does not necessarily translate into improved inhibition of both cholinesterases. PBO-10 exhibited comparatively lower activity against both enzymes, suggesting that excessive steric bulk or an unfavorable molecular orientation may limit productive binding. Overall, the SAR analysis indicates that relatively small and moderately lipophilic substituents can favor AChE inhibition, whereas smaller halogen substitution, particularly fluorine, appears beneficial for BChE inhibition. However, the enzyme-dependent activity patterns demonstrate that substituent effects are not governed solely by electronic properties or lipophilicity, but likely reflect the distinct structural environments of the AChE and BChE active sites.

Structure-Based Interpretation of Molecular Docking Results

The molecular docking results provided a structural rationale for the experimentally observed inhibitory activities of the most active derivatives. In the hAChE docking analysis, PBO-5, which exhibited the strongest experimental AChE inhibition (IC_{50} = 0.537 µM), showed a favorable docking score of -9.08 kcal/mol and adopted a binding orientation within the active-site gorge. As illustrated in Figure 5, PBO-5 was surrounded by Tyr124, Glu202, Phe338, Tyr341, and His447. These residues represent structurally distinct regions of the gorge rather than a single catalytic site. Tyr124 is located in the upper region of the gorge and has been implicated in ligand recognition, whereas Phe338 and Tyr341 are aromatic residues lining the active-site gorge and can contribute to hydrophobic and aromatic interactions. His447 forms part of the catalytic triad together with Ser203 and Glu334. The proximity of PBO-5 to these residues therefore suggests that its binding orientation is compatible with occupation of the functionally important region of the hAChE gorge. Previous mutagenesis and structural studies have shown that aromatic gorge residues, including Tyr124, Phe338, and Tyr341, are important for recognizing cholinesterase inhibitors.[28]

Importantly, the experimental SAR cannot be attributed solely to the calculated docking score. Although PBO-5 showed substantially stronger experimental AChE inhibition than the unsubstituted PBO-1 (IC_{50} = 0.537 versus 6.520 µM), its calculated docking score was slightly less favorable than that of PBO-1 (-9.08 versus -9.39 kcal/mol). This discrepancy highlights the limitations of interpreting docking scores as direct predictors of experimental potency. Nevertheless, the docking pose of PBO-5 indicates that the para-methyl-substituted aryl group can be accommodated within the aromatic-rich gorge and establish favorable non-covalent contacts.

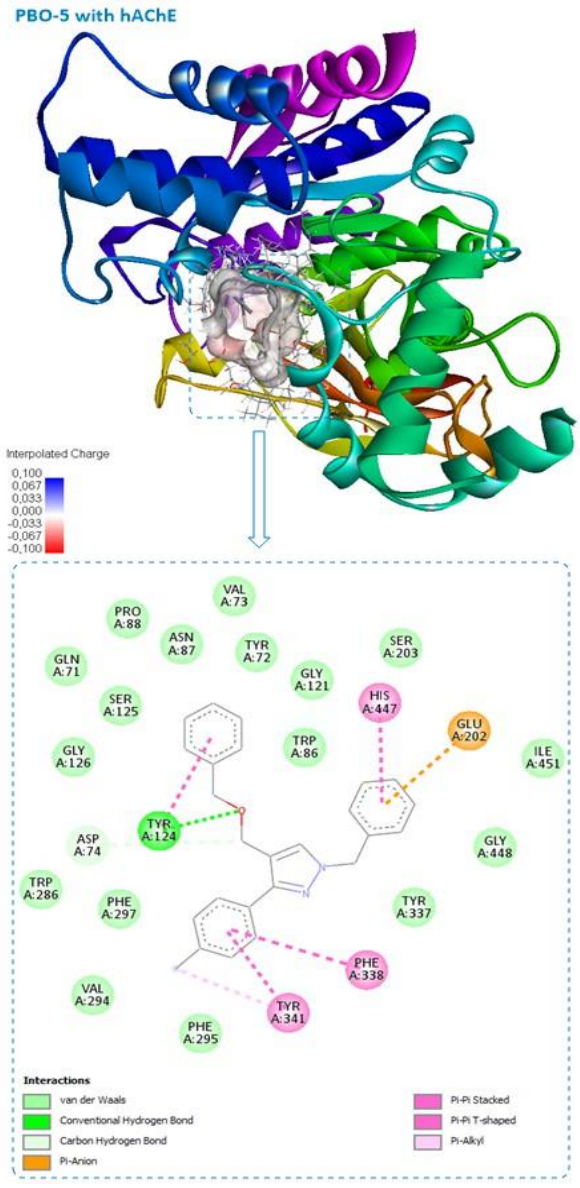

Figure 5. 2D and 3D binding interactions of PBO-5 within the active site of hAChE (PDB ID: 7E3H).

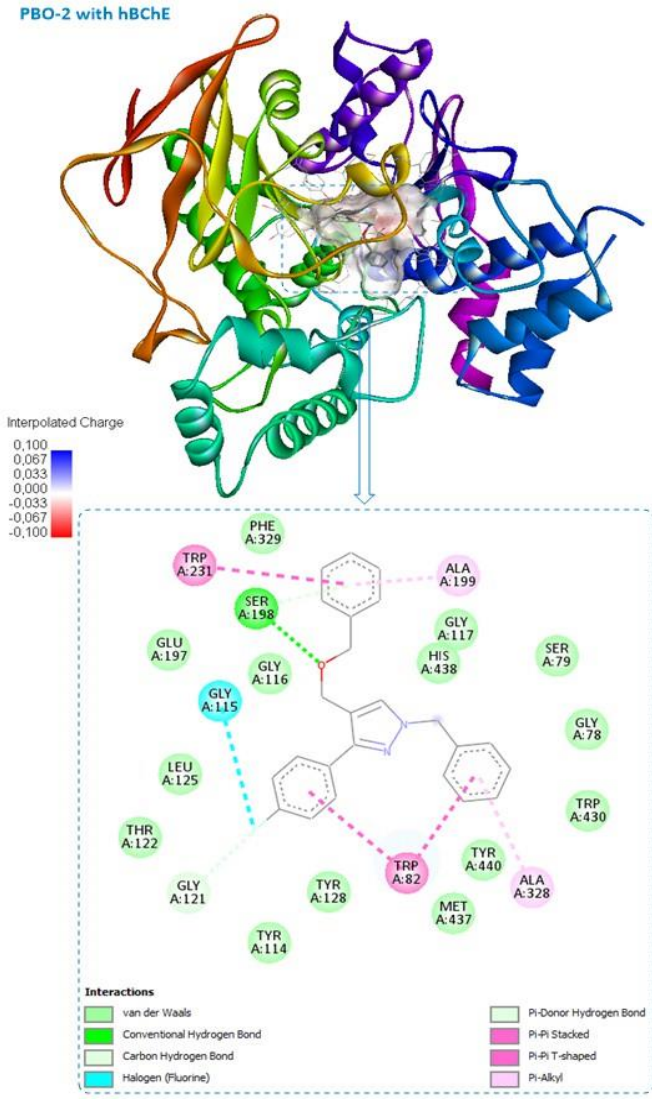

Figure 6. 2D and 3D binding interactions of PBO-2 within the active site of hBChE (PDB ID: 4BDS).

For hBChE, PBO-2 was identified as the most active experimental inhibitor (IC_{50} = 0.958 µM). The compound adopted a binding orientation within the active-site gorge and contacted Trp82, Gly115, Gly121, Ser198, Ala199, Trp231, and Ala328 (Figure 6). These residues represent several functionally important regions of the BChE gorge. Trp82 forms the principal anionic/choline-binding subsite and is a recurrent aromatic anchoring residue for BChE inhibitors, whereas Ser198 belongs to the catalytic triad together with Glu325 and His438. The presence of PBO-2 in this functionally dense region of the gorge therefore suggests that its inhibitory activity may arise from simultaneous stabilization through aromatic and hydrophobic contacts with the catalytic gorge.

A structural comparison of the two cholinesterases further provides a framework for interpreting the different activity profiles of the PBO derivatives. Although AChE and BChE share conserved catalytic machinery and an aromatic-rich active-site gorge, their peripheral and acyl-binding regions differ substantially. In hAChE, Phe295 and Phe297 contribute to a relatively restricted acyl pocket, whereas the corresponding BChE gorge is more permissive to bulky substituents.[26] Structural studies of cholinesterase inhibitors have further shown that Trp86 in AChE and Trp82 in BChE provide conserved aromatic anchoring sites, while differences in surrounding residues influence ligand orientation and accommodation.[28] These structural differences may contribute to the distinct SAR observed for the PBO series against hAChE and hBChE.

The relatively low intra-cluster RMSD values indicate that the docking protocol generated closely related poses within the corresponding solution clusters, although these values should not be interpreted as an independent measure of agreement with experimentally determined ligand conformations. Taken together, the experimental SAR and docking analyses suggest that variation in the nature and steric properties of the aryl substituent may influence the ability of these pyrazole derivatives to adopt favorable orientations within the distinct binding environments of hAChE and hBChE. The docking results therefore provide a structural hypothesis that complements, rather than independently establishes, the experimentally observed SAR.

The present study has several limitations. Inhibition was measured with *Electrophorus electricus* AChE and equine serum BChE, whereas docking was performed on the human enzymes. Given differences between these species in the residues lining the active-site gorge and the peripheral site, interpret the docking results cautiously. The predicted poses may help explain the observed SAR but do not establish the involvement of specific residue contacts. The IC_{50} values were obtained from technical triplicates, which do not capture variability between independent experiments. The mode of inhibition and the K_i values were not determined, and no cytotoxicity, permeability, or metabolic stability data were collected. Additionally, although PBO-2 showed the strongest experimental BChE inhibition, its docking score (-7.86 kcal/mol) was not the most favorable among the investigated compounds, indicating that docking scores did not directly correspond to the experimentally determined inhibitory potency. These findings should therefore be interpreted within the context of the enzyme sources and assay conditions used, and further studies are needed to assess their relevance to human enzymes and biological systems.

In conclusion, a series of hybrid pyrazole derivatives was successfully synthesized and characterized, and their cholinesterase inhibitory activities were evaluated. PBO-5 exhibited the strongest AChE inhibition (IC_{50} = 0.537 µM), whereas PBO-2 showed the highest BChE inhibition (IC_{50} = 0.958 µM). The combined SAR and molecular docking analyses provided complementary structural insights into the observed inhibitory profiles, with PBO-5 and PBO-2 emerging as compounds of interest for further investigation and optimization.

Ethics Committee Approval: This study did not require ethics committee approval because no human or animal subjects were used.
Informed Consent: Not applicable, as this study does not involve human participants or animal experiments.
Author Contributions: Concept - B.K., F.D.; Design - B.K.; Supervision - B.K.; Resources – B.K., F.D.; Data Collection and/or Processing- B.K., B.N.K., F.D.; Analysis and/or Interpretation – B.K., F.D.; Literature Search – B.K.; Writing Manuscript – B.K., F.D.; Critical Review – B.K., F.D.
Conflict of Interest: The authors have no conflicts of interest to declare.
Financial Disclosure: This study was supported by the Van Yuzuncu Yil University Scientific Research Projects Coordination Unit (BAP) under project number THD-2026-13003.
Use of Artificial Intelligence: AI tools were used solely for language editing.

REFERENCES

1. Safiri S, Jolfayi GA, Fazlollahi A, et al. Alzheimer's disease: a comprehensive review of epidemiology, risk factors, symptoms diagnosis, management, caregiving, advanced treatments and associated challenges. *Front Med.* 2024;11:1474043. [CrossRef]
2. Abdulkhaliq AA, Kim B, Almoghrabi YM, et al. Amyloid-β and Tau in Alzheimer's disease: pathogenesis, mechanisms, and interplay. *Cell Death Dis.* 2026;17(1):21. [CrossRef]
3. Chen ZR, Huang JB, Yang SL, Hong FF. Role of cholinergic signaling in Alzheimer's disease. *Molecules.* 2022;27(6):1816. [CrossRef]
4. Marucci G, Buccioni M, Dal Ben D, Lambertucci C, Volpini R, Amenta F. Efficacy of acetylcholinesterase inhibitors in Alzheimer's disease. *Neuropharmacology.* 2021;190:108352. [CrossRef]
5. Lane RM, Potkin SG, Enz A. Targeting acetylcholinesterase and butyrylcholinesterase in dementia. *Int J Neuropsychopharmacol.* 2006;9(1):101-124. [CrossRef]
6. Prešern U, Goličnik M, Bavec A. Genetic and functional dynamics of butyrylcholinesterase in Alzheimer's disease: From mechanisms to clinical relevance. *Chem Biol Interact*. 2025;423:111809. [CrossRef]
7. Balson R, Gibson PR, Ames D, Bhathal PS. Tacrine-induced hepatotoxicity: tolerability and management. *CNS Drugs.* 1995;4(3):168-181. [CrossRef]
8. Rountree SD, Atri A, Lopez OL, Doody RS. Effectiveness of antidementia drugs in delaying Alzheimer's disease progression. *Alzheimers Dement.* 2013;9(3):338-345. [CrossRef]
9. Zhang J, Zhang Y, Wang J, Xia Y, Zhang J, Chen L. Recent advances in Alzheimer's disease: mechanisms, clinical trials and new drug development strategies. *Signal Transduct Target Ther.* 2024;9(1):211. [CrossRef]
10. Silva MA, Kiametis AS, Treptow W. Donepezil inhibits acetylcholinesterase via multiple binding modes at room temperature. *J Chem Inf Model.* 2020;60(7):3463-3471. [CrossRef]
11. Sugimoto H, Yamanish Y, Iimura Y, Kawakami Y. Donepezil hydrochloride (E2020) and other acetylcholinesterase inhibitors. *Curr Med Chem.* 2000;7(3):303-339. [CrossRef]
12. Kareem RT, Abedinifar F, Mahmood EA, Ebadi AG, Rajabi F, Vessally E. The recent development of donepezil structure-based hybrids as potential multifunctional anti-Alzheimer's agents: highlights from 2010 to 2020. *RSC Adv.* 2021;11(49):30781-30797. [CrossRef]
13. van Greunen DG, van der Westhuizen CJ, Cordier W, et al. Novel N-benzylpiperidine carboxamide derivatives as potential cholinesterase inhibitors for the treatment of Alzheimer's disease. *Eur J Med Chem.* 2019;179:680-693. [CrossRef]
14. Saeedi M, Felegari P, Iraji A, et al. Novel N-benzylpiperidine

derivatives of 5-arylisoxazole-3-carboxamides as anti-Alzheimer's agents. *Arch Pharm.* 2021;354(3):2000258. [CrossRef]
15. Neshat N, Hashmi Z, Islam R, et al. Indole-based heterocyclic conjugates: design, synthesis, *in silico* studies and cholinesterase inhibition. *J Mol Struct.* 2025;1319:139529. [CrossRef]
16. Pourtaher H, Hasaninejad A, Iraji A. Design, synthesis, *in silico* and biological evaluations of novel polysubstituted pyrroles as selective acetylcholinesterase inhibitors against Alzheimer's disease. *Sci Rep.* 2022;12(1):15236. [CrossRef]
17. Al-Maqtari HM, Hasan AH, Suleiman M, et al. Benzyloxychalcone hybrids as prospective acetylcholinesterase inhibitors against Alzheimer's disease: rational design, synthesis, *in silico* ADMET prediction, QSAR, molecular docking, DFT, and molecular dynamic simulation studies. *ACS Omega.* 2024;9(30):32901-32919. [CrossRef]
18. Gabr M, Murugan NA. Discovery of biphenyl pyrazole scaffold for neurodegenerative diseases: a novel class of acetylcholinesterase-centered multitargeted ligands. *Bioorg Med Chem Lett.* 2020;30(17):127370. [CrossRef]
19. Pizzo C, Faral-Tello P, Yaluff G, et al. New approach towards the synthesis of selenosemicarbazones, useful compounds for Chagas' disease. *Eur J Med Chem.* 2016;109:107-113. [CrossRef]
20. Lebedev AV, Lebedeva AB, Sheludyakov VD, Kovaleva EA, Ustinova OL, Kozhevnikov IB. Synthesis of 3-substituted arylpyrazole-4-carboxylic acids. *Russ J Gen Chem.* 2005;75:782-789. [CrossRef]
21. Karcı BN, Çöven FO, Ergüç A, Kuzu B. VEGFR-2 targeting oxadiazole-pyrazole hybrids: synthesis, molecular docking, and cytotoxic evaluation in cancer cells. *ChemistrySelect.* 2026;11(16):e73346. [CrossRef]
22. Deniz E, Çöven FO, Ergüç A, Karakuş F, Kuzu B. Design, synthesis, and evaluation of benzoxazole-linked pyrazole hybrids as VEGFR-2-targeted antiproliferative agents. *Cell Biochem Biophys.* 2025;83:4961-4975. [CrossRef]
23. Arzuk E, Pinar İ, Kuzu B. Synthesis and biological evaluation of benzyloxymethyl-substituted imidazo[1,2-a]pyridines as apoptosis-inducing anticancer agents through modulation of BCL-2/Bax signaling and caspase-3 activation. *Naunyn Schmiedebergs Arch Pharmacol.* 2026;399:19537-19554. [CrossRef]
24. Ellman GL, Courtney KD, Andres V Jr, Featherstone RM. A new and rapid colorimetric determination of acetylcholinesterase activity. *Biochem Pharmacol.* 1961;7(2):88-95. [CrossRef]
25. Dileep KV, Ihara K, Mishima-Tsumagari C, et al. Crystal structure of human acetylcholinesterase in complex with tacrine: implications for drug discovery. *Int J Biol Macromol*. 2022;210:172-181. [CrossRef]
26. Nachon F, Carletti E, Ronco C, et al. Crystal structures of human cholinesterases in complex with huprine W and tacrine: elements of specificity for anti-Alzheimer's drugs targeting acetyl- and butyryl-cholinesterase. *Biochem J*. 2013;453(3):393-399. [CrossRef]
27. Kuzu B, Demir Y. Synthesis of novel pyrazino[1,2-a]indol-1(2H)-one derivatives as potent cholinesterase inhibitors and their *in vitro* and *in silico* evaluations. *Arch Biochem Biophys.* 2025;771:110504. [CrossRef]
28. Ordentlich A, Barak D, Kronman C, et al. Dissection of the human acetylcholinesterase active center determinants of substrate specificity. Identification of residues constituting the anionic site, the hydrophobic site, and the acyl pocket. *J Biol Chem*. 1993;268(23):17083–17095. [CrossRef]